The Holocene 8,3 (1998) pp. 331–339

Luminescence dating of recent dunes on Inch Spit, Dingle Bay, southwest Ireland

A.G. Wintle,[1] M.L. Clarke,[2] F.M. Musson,[1] J.D. Orford[3] and R.J.N. Devoy[4]

([1]Institute of Geography and Earth Sciences, University of Wales, Aberystwyth, Ceredigion SY23 3DB, Wales, UK; [2]Department of Geography, University of Nottingham, University Park, Nottingham NG7 2RD, UK; [3]School of Geosciences, Queen's University, Belfast, Northern Ireland, BT7 1NN, UK; [4]Department of Geography, University College Cork, College Road, Cork, Ireland)

Received 19 February 1997; revised manuscript accepted 9 September 1997

A HOLOCENE RESEARCH PAPER

Abstract: Fifteen samples of dune sand, and three samples from a core taken in the beach face, were collected from a sand spit which protrudes into Dingle Bay in Southwest Ireland. The potassium-rich feldspar grains from the samples were dated using a single aliquot luminescence protocol for infrared stimulated luminescence (IRSL) signals. No ages over 600 years were obtained, which demonstrates the youth of the dune forms currently observed. The youngest ages were about 150 years old, but for these samples the scatter in the equivalent dose obtained as the mean of 18 measurements was higher than for the older samples.

Key words: Luminescence, IRSL, optical dating, dunes, Dingle, Ireland.

Introduction

All luminescence dating techniques rely on the trapping of charge (e.g. electrons) in crystals following their exposure to ionizing radiation, such as the alpha, beta and gamma radiation produced during decay of naturally occurring radioactive isotopes (primarily uranium, thorium and potassium). In the laboratory the charge is released from the traps and recombines within the crystals with the release of energy, some of which occurs as luminescence; if thermal energy is applied to release the charge, then thermoluminescence (TL) is produced. If the energy is in the form of photons, then optically stimulated luminescence is produced, with several different optical dating methods being reported (Wintle, 1993).

Optical dating methods are better suited to sediments deposited in the last 5000 years than methods based upon the TL from the same minerals because all of the signal is light-sensitive, whereas only part of the TL signal is light-sensitive, and thus retains a residual signal at deposition. The primary advantage is that mineral grains, primarily quartz and feldspar from modern sediments give an optically stimulated luminescence signal which cannot be seen above the intrinsic noise level of the luminescence detection system, whereas the TL signal from the same grains will be finite and substantially above the intrinsic noise level. It is thus more difficult to determine an increase in the TL signal brought about by subsequent exposure of the grains to radiation from their immediate environment.

Several types of optical dating methods have been reported in the literature. A green line (514.5 nm) from an argon ion laser has been used to stimulate luminescence from quartz (e.g. Stokes, 1992; Pye *et al.*, 1995). Infrared-emitting diodes have been used to obtain infrared-stimulated luminescence (IRSL) from feldspars (Edwards, 1993). Dating of inland dune systems in the USA has been carried out using the OSL of quartz (Stokes and Gaylord, 1993) and using IRSL of potassium-rich feldspars (Edwards, 1993; Clarke, 1994; Clarke *et al.*, 1996). The results of these studies have shown ages consistent with stratigraphy, and agree with the radiocarbon age control (Clarke, 1994; Stokes and Gaylord, 1993). The success of IRSL dating of sands from the Mojave Desert and the demonstration of the ability of this method to provide ages as young as a few hundred years for dune deposition (Edwards, 1993; Clarke *et al.*, 1996) led to its use in the current study. The potential for coastal dune sands was further demonstrated by Ollerhead *et al.* (1994) who used diode-stimulated IRSL from potassium-rich feldspars separated from five samples of sand from a dune sequence on Buctouche Spit, New Brunswick, Canada. Ages in the range of 5 ± 30 to 765 ± 45 years were obtained for the dunes along the length of the spit, which was originally

0959-6836(98)HL245RP

thought to have formed some time in the last 5000 years (Ollerhead and Davidson-Arnott, 1995).

Inch Spit dune complex

In Ireland, sand dunes occur on around 20% of the coastline, covering an area of over 160 km^2 (Carter, 1990). Coastal dune formation is thought to result from the interaction between sea-level change and sediment supply, with the majority of dunes formed within the last 6000 years (Carter *et al.*, 1989). The dunes on the west coast of Ireland tend to form between headlands and in estuarine embayments, due to high-energy incident waves and onshore winds. The dune spits at Inch and Rossbeigh, County Kerry, formed in a high sand supply environment created by the conjunction of tidal and aeolian processes, termed by Carter (1990) a 'tidal pump' system. High accretion rates, resulting from sediment cycling between beach, dune and tidal estuary, limit vegetation stabilization and therefore there is no sedimentary evidence of surface stability and palaeosol formation within the dunes.

Inch Spit progrades into Dingle Bay from the northern shore (Figure 1) for a distance of about 5 km, lying normal to the dominant Atlantic westerly winds. At the northern, landward end, the Atlantic-facing beach grades into a foredune, about 6 m in height, which is currently undergoing active erosion. From about 2 km away from the landward end to its distal point, five smaller foredune ridges are interposed between the large dune, here up to 20 m high, and the beach. The large dune marks the seaward end of the main dune complex, which covers an area of 1250 ha (Figure 2). Five parabolic dunes (labelled A to E in Figure 3) orientated east–west cut across the spit indicating postdepositional wind erosion and sand reactivation, with the blowouts now forming interdune areas of vegetation colonization at, or just above, the water table. The main dune complex is currently stabilized by marram grass.

This paper describes a project to apply luminescence dating to the sand dunes on Inch Spit to obtain a chronology for sand accumulation. An independent chronology has been obtained from radiocarbon dating of shells associated with parabolic dune E. Whole oyster shells underlying small wave refraction-controlled wave-lain gravel ridges, protruding from under the parabolic dune side-wall, gave a calibrated ^{14}C date between 1150 and 1050 years BP ($\pm 2\sigma$ range: UB-3819). A midden horizon of burnt mollusc shells emerging from the trailing back of a parabolic dune gave a calibrated ^{14}C date between 500 and 340 years BP ($\pm 2\sigma$ range: UB-3970).

Sample collection, preparation and analytical procedures

Five luminescence samples were taken from the main dune ridge along the length of the spit (labelled A1, B1, C1, D1 and E1 in Figure 3). The heights of the samples were levelled to OD Belfast using a Sokkia total station. Samples B2–B7 were taken from a transect cutting across the main dune ridge (B2–B5), the foredune (B6–B7) and including a borehole within the upper beach (B8/1–B8/3; Figure 4). The remaining samples were taken from the side arm of parabolic dune E, which is the southernmost parabolic dune on the spit.

Samples from parabolic dune side-wall locations were collected in the field by hammering in lengths of black plastic drainpipe that prevented sunlight exposure. All side-wall samples were taken from faces which showed low-angle landward-dipping beds of the parabolic dunes. Subsurface samples were collected by augering into the base of a small pit which was covered by a black tarpaulin during sampling. Beach face samples were taken with a large-diameter auger.

Dosimetry measurements were made upon a dried subsample of the bulk sediment (Table 1). About 20 g of this was ground in a steel ball mill to a diameter of less than 10 μm and the external alpha and beta contributions to the total dose rate measured using a Daybreak 582 Alpha Counter and a SURRC Thick Source Beta Counter (Sanderson, 1988). For beta counting, Shap Granite was used as a standard (6.25 Gy/ka) and magnesium oxide as the back-

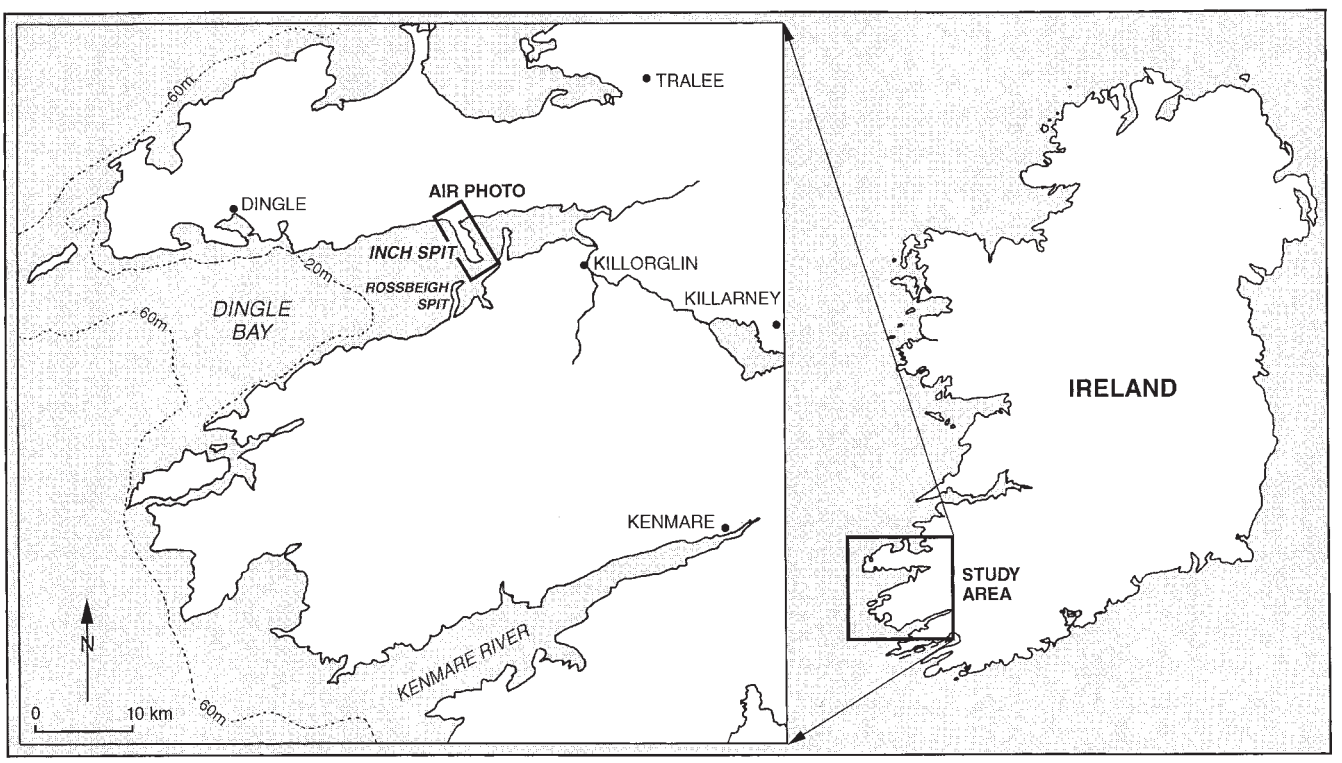

Figure 1 Location of Inch Spit.

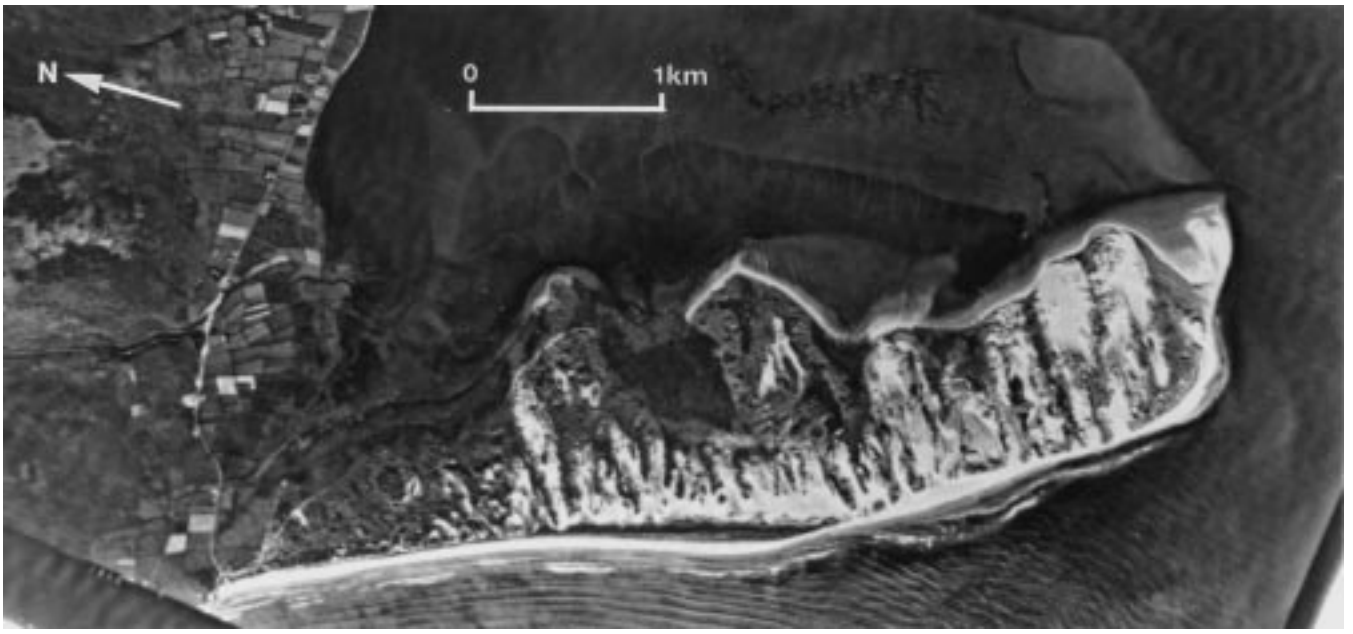

Figure 2 1973 airphoto of Inch, identifying parabolic dune activity.

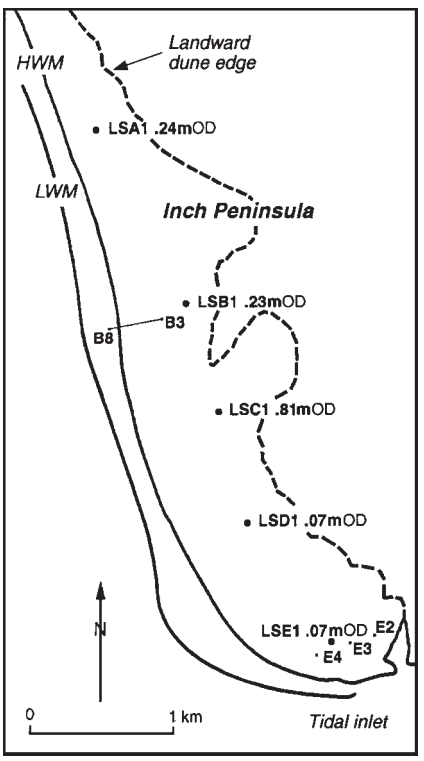

Figure 3 Location map of samples A1–E1, B3–B8 and E2–E4.

ground (0 Gy/ka). Both sealed and unsealed alpha counting was employed and the count rates obtained were ±5% of each other, indicating no radon loss from the samples. Slow pair counting was employed to calculate concentrations of uranium and thorium.

For most samples the grain size fraction 180–210 μm made up 50–70% of the bulk and this size fraction was selected from a bulk sample by sieving. Carbonates and organics were removed from the sand fraction by washing in 0.0032 M HCl and 30% H_2O_2. The potassium-rich feldspar grains used in IRSL measurement were obtained from the sand by density separation using sodium polytungstate. All procedures were carried out in dim orange light conditions to prevent IRSL signal depletion. The grains were not etched with hydrofluoric acid and the contribution to the total dose rate from external alpha irradiation was calculated using an alpha attenuation value of 0.2 ± 0.1. The internal beta dose rate was calculated from the potassium content of a 100 mg subsample of the potassium feldspar separates used in luminescence measurement. The potassium content was determined on a Risø GM multicounter system (Bøtter-Jensen and Mejdahl, 1985) using potassium feldspar (NIST 70a) and magnesium oxide as standards.

The cosmic dose to the sample was calculated using the formula of Prescott and Hutton (1988) together with the current burial depth, or estimated depth for those samples from the base of the current interdune corridors. The external gamma contribution was measured in the field (Table 1) using an NE Technology PSR8 gamma scintillator with a 2-inch sodium iodide detector. For all samples the bulk potassium content was calculated from the alpha dose rate and the infinite beta dose rate and is given in Table 1. For samples below the current water table, either in the interdune corridors or in the core from the beach, field gamma measurements could not be made and the gamma dose rates were estimated from the laboratory data.

Water contents were measured for the dune samples as collected (Table 1) and varied from 2.5 to 22.5% (wet weight), with the higher values being obtained for those collected from below the surface of the interdune corridors. Rather than use the individual values in the age calculations, the water content and its likely annual range through time since burial was estimated on the basis of its field position (Table 2); those taken high in the sides of the dune corridors were likely to have been well drained throughout (5 ± 5%), and those from below the present water table were likely to have been in a similar condition since deposition (20 ± 5 or 15 ± 5%). Estimated higher water contents (30 ± 10% of wet sediment) were used for samples from below current sea level (B8/1 to B8/3) because of loss of water as the samples were extracted.

The various dose rate contributions, allowing for grain size attenuation and absorption of part of the dose by the water in the sediment, were calculated using the age program written by R. Grün, using the dose rate values of Nambi and Aitken (1986), and are given in Table 2. Using the total dose rate and the mean Equivalent Dose (ED) obtained for each sample using IRSL measurements, the age for each sample was calculated.

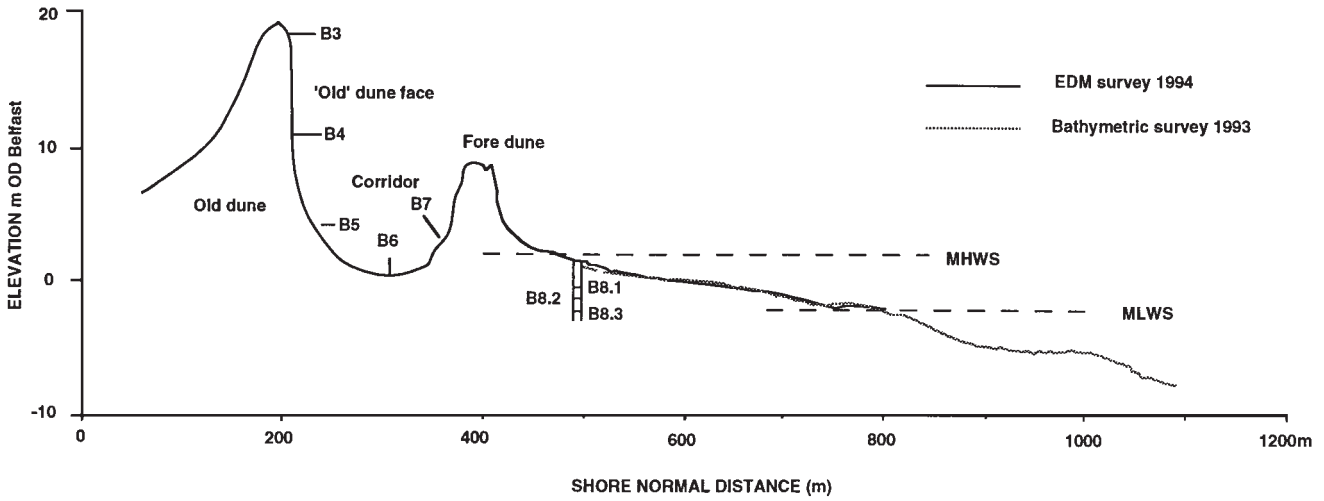

Figure 4 Schematic cross-section to show B3–B7 and B8/1–B8/3.

Table 1 Radioactivity measurements and related data

Sample	Measured water content (%)	Uranium (ppm)	Thorium (ppm)	Alpha count rate (cts/ks/cm^2)	Infinite beta dose (Gy/ka)	Calculated K%	Field gamma dose rate (μGy/a)
A1	22.5	0.76 ± 0.13	2.18 ± 0.42	0.167 ± 0.005	0.54 ± 0.03	0.45	n/d
B1a	4.5	0.92 ± 0.13	1.46 ± 0.42	0.161 ± 0.006	0.46 ± 0.05	0.35	n/d
B1	17.0	0.73 ± 0.19	3.38 ± 0.63	0.206 ± 0.006	0.61 ± 0.06	0.50	262 ± 16
B2	3.0	0.74 ± 0.02	2.21 ± 0.67	0.166 ± 0.007	0.60 ± 0.03	0.53	279 ± 17
B3	2.5	0.84 ± 0.13	1.43 ± 0.04	0.150 ± 0.005	0.44 ± 0.03	0.34	316 ± 19
B4	4.0	0.33 ± 0.18	3.34 ± 0.58	0.157 ± 0.005	0.51 ± 0.04	0.45	271 ± 16
B5	4.0	1.34 ± 0.15	2.17 ± 0.46	0.235 ± 0.006	0.54 ± 0.07	0.35	298 ± 18
B6	13.5	2.18 ± 0.23	2.70 ± 0.72	0.354 ± 0.010	0.64 ± 0.13	0.30	301 ± 18
B7	6.0	0.79 ± 0.09	3.07 ± 0.58	0.202 ± 0.006	0.66 ± 0.05	0.56	332 ± 20
C1	20.0	0.91 ± 0.11	1.35 ± 0.11	0.156 ± 0.005	0.55 ± 0.04	0.46	n/d
D1	21.5	0.96 ± 0.13	2.00 ± 0.04	0.184 ± 0.006	0.47 ± 0.05	0.33	n/d
E1	18.0	0.87 ± 0.13	1.56 ± 0.51	0.158 ± 0.006	0.40 ± 0.08	0.28	n/d
E2	6.0	0.95 ± 0.10	0.89 ± 0.27	0.144 ± 0.005	0.38 ± 0.04	0.26	252 ± 15
E3	4.0	0.68 ± 0.15	2.54 ± 0.49	0.170 ± 0.005	0.40 ± 0.09	0.28	303 ± 18
E4 beachface	4.0	0.88 ± 0.12	1.37 ± 0.37	0.153 ± 0.005	0.53 ± 0.07	0.40	255 ± 15
B8/1	n/d	2.30 ± 0.24	4.37 ± 0.76	0.428 ± 0.010	0.85 ± 0.07	0.48	n/d
B8/2	n/d	0.97 ± 0.12	2.26 ± 0.37	0.195 ± 0.005	0.50 ± 0.05	0.36	n/d
B8/3	n/d	0.88 ± 0.13	1.38 ± 0.41	0.154 ± 0.006	0.39 ± 0.04	0.27	n/d

Table 2 Attenuated dosimetry data and calculated ages

Sample	Water content (%)	Internal K%	Internal beta dose (μGy/a)	External alpha dose (μGy/a)	External beta dose (μGy/a)	External gamma dose (μGy/a)	Cosmic dose (μGy/a)	Total dose rate (μGy/a)	ED (Gy)	Age (years)
A1	20 ± 5	7.5 ± 0.8	493 ± 61	66 ± 35	327 ± 34	280 ± 30	185 ± 19	1310 ± 80	0.78 ± 0.05	595 ± 52
B1a	5 ± 5	9.3 ± 0.9	504 ± 61	84 ± 43	391 ± 49	270 ± 30	185 ± 19	1431 ± 96	0.21 ± 0.03	147 ± 23
B1	20 ± 5	4.5 ± 0.4	244 ± 28	82 ± 43	421 ± 52	262 ± 30	185 ± 19	1194 ± 82	0.42 ± 0.05	352 ± 48
B2	5 ± 5	7.3 ± 0.7	395 ± 48	84 ± 44	510 ± 42	279 ± 30	185 ± 19	1453 ± 113	0.22 ± 0.03	151 ± 23
B3	5 ± 5	8.2 ± 0.8	444 ± 54	75 ± 40	374 ± 35	316 ± 30	185 ± 19	1395 ± 84	0.29 ± 0.07	208 ± 51
B4	5 ± 5	8.5 ± 0.8	460 ± 45	80 ± 43	433 ± 44	271 ± 30	164 ± 12	1408 ± 83	0.32 ± 0.03	227 ± 25
B5	5 ± 5	8.7 ± 0.8	475 ± 56	118 ± 62	458 ± 66	298 ± 30	116 ± 17	1466 ± 111	0.54 ± 0.03	368 ± 34
B6	10 ± 5	8.4 ± 0.8	455 ± 55	152 ± 79	474 ± 35	301 ± 30	184 ± 19	1567 ± 110	0.52 ± 0.03	332 ± 30
B7	5 ± 5	3.2 ± 0.3	173 ± 21	102 ± 54	560 ± 56	332 ± 35	185 ± 19	1353 ± 90	0.44 ± 0.04	325 ± 36
C1	20 ± 5	8.7 ± 0.9	471 ± 60	62 ± 33	379 ± 62	280 ± 30	185 ± 19	1376 ± 86	0.19 ± 0.02	138 ± 16
D1	20 ± 5	8.1 ± 0.8	439 ± 54	73 ± 40	324 ± 58	280 ± 30	185 ± 19	1301 ± 86	0.19 ± 0.02	146 ± 18
E1	20 ± 5	9.5 ± 1.0	514 ± 66	63 ± 34	276 ± 68	280 ± 30	185 ± 19	1318 ± 101	0.66 ± 0.03	501 ± 44
E2	5 ± 5	7.4 ± 0.7	451 ± 55	72 ± 13	323 ± 40	252 ± 30	185 ± 19	1233 ± 81	0.44 ± 0.03	357 ± 33
E3	5 ± 5	9.1 ± 0.9	493 ± 60	93 ± 49	403 ± 75	303 ± 30	185 ± 19	1404 ± 116	0.73 ± 0.04	520 ± 51
E4 beachface	5 ± 5	8.5 ± 0.9	460 ± 60	77 ± 40	382 ± 80	255 ± 26	185 ± 19	1427 ± 103	0.38 ± 0.06	266 ± 46
B8/1	30 ± 10	9.3 ± 1.0	50566	141 ± 77	502 ± 91	392 ± 72	197 ± 10	1733 ± 154	0.37 ± 0.03	213 ± 25
B8/2	30 ± 10	8.2 ± 0.9	442 ± 63	64 ± 35	286 ± 58	202 ± 37	151 ± 8	1155 ± 100	0.53 ± 0.04	459 ± 52
B8/3	30 ± 10	9.1 ± 1.0	495 ± 65	51 ± 28	231 ± 44	150 ± 27	135 ± 7	1062 ± 88	0.54 ± 0.04	509 ± 56

Luminescence measurements and discussion of ED determinations

Luminescence measurements were undertaken using a Risø Automated TL-OSL Reader with stimulation using an array of 12 infrared diodes with a peak emission at 880±80 nm. The stimulated luminescence from the sample passed through a Schott BG39 colour glass filter to reject the output from the diodes, and was detected by an EMI 9635QA photomultiplier tube. Stimulation was for 0.5 s and background counts for the measurements were less than 20 counts in this time period; this was subtracted from each IRSL measurement prior to data analysis. Natural IRSL intensities (i.e. brightness) of the aliquots obtained after a preheat of 220°C for 10 minutes from the youngest to the oldest sample ranged from 254 (cts in 0.5 s) for sample C to 2443 (cts in 0.5 s) for sample A.

The Equivalent Dose (ED) was determined using a single aliquot additive dose method applied to each of 18 discs, using the following sequence of measurements: a preheat of 220°C for 10 minutes; 0.5-second IR stimulation at 50°C; irradiation within the reader from a $^{90}Sr/^{90}Y$ beta source; followed by further preheat and measurement etc. Another six discs were used to calibrate for loss of signal due to repetitive preheat and measurement (Figure 5) by employing the same procedure as above, but without giving any irradiation. Using the calibrated additive dose run, a 'growth curve' of signal intensity with increasing radiation dose is created (Figure 6) and the ED can be determined by extrapolation back to the dose axis. The repeat points shown in Figure 6 are used as a cross check on the efficiency of the calibration procedure and should fall on a horizontal line across from the top dose point. Eighteen ED determinations are produced for each sample and the mean of at least 15 of these is used in the age calculation (Table 2).

In the single aliquot procedure, the ED is produced by constructing a growth curve for each aliquot, the slope of which is the IRSL sensitivity of the grains in that aliquot (Duller, 1991; 1995). Growth curves are shown (Figure 7) for single aliquots from the oldest (A1) and youngest (C1) samples in this study. Comparison of the slopes shows that the average sensitivity of the grains within each aliquot is similar. The intercept of the lines with the dose axis gives the ED for each sample. For each aliquot the ED is obtained with the precision indicated by the fit (0.70 ± 0.02 Gy for A1 (vi) and 0.16 ± 0.01 Gy for C1 (vi)).

The use of the single aliquot procedure has several advantages over the multiple aliquot procedure, in which individual aliquots are given different radiation doses ranging from zero to several times their expected ED, preheated and then measured. An important advantage is that the ED is determined for 18 independent samples, which are combined for the ED used in the age calculation. Table 3 gives the ED and natural IRSL intensity, I_n, for all discs for samples A1 and C1. The fitting error varies from 2 to 13% for sample A1; for the ED used in the age calculation, discs 1, 5 and 14 were omitted due to poor visual fitting of the data points. The calculated ED is the mean of the 15 individual deteminations and the error is expressed as the standard deviation from the mean, σ; for A1, ED = 0.78 ± 0.05 Gy and for C1, ED = 0.185 ± 0.02 Gy. (NB If the statistical error on the mean $\sigma/\sqrt{n}$ is used, ED = 0.78 ± 0.01 (n = 15).)

Use of a single aliquot procedure does not require inter-aliquot normalization, as needed by Ollerhead *et al.* (1994) in the multiple aliquot procedure, to reduce scatter from 17% to 6% for the 20 discs that they used. For well-bleached grains (i.e. those which have had their IRSL signal erased by exposure to sunlight at deposition and those from an environment in which they received an identical radiation dose) the value of the ED obtained for each aliquot will be identical within the measurement error. Some spread in ED values is obtained even for the 18 aliquots of B6, as shown in Figure 8. The values of ED given in Table 2 are the mean and standard deviation. Had a multiple aliquot method been used, the non-identical nature of each aliquot would have shown

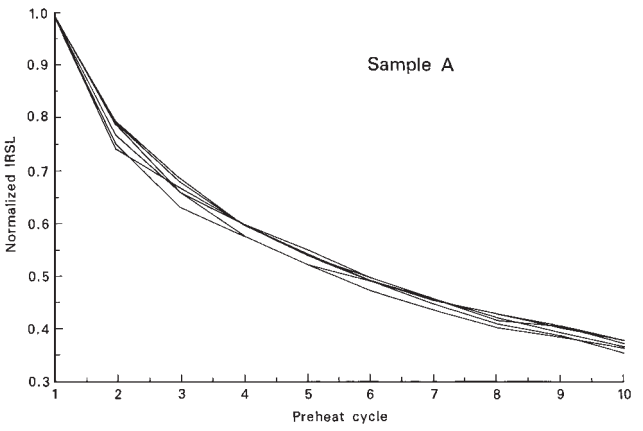

Figure 5 Calibration curve to permit correction of additive dose points after each calibration cycle involving preheating at 220°C for 10 minutes. Data are for six discs of sample A1. In the interests of clarity, individual data points for each cycle are not shown, but are linked with straight lines to show trend of depletion.

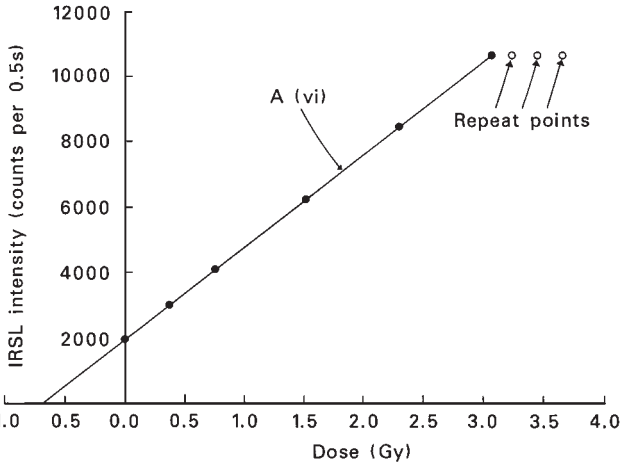

Figure 6 Growth curve of IRSL intensity (counts obtained in 0.5 s) for disc 6 (vi) of sample A1 as a function of laboratory dose; extrapolation to dose axis gives ED = 0.68 ± 0.02 Gy, as given in Table 3. Repeat points are identical to final point with added dose of 3 Gy, indicating appropriateness of correction for each cycle.

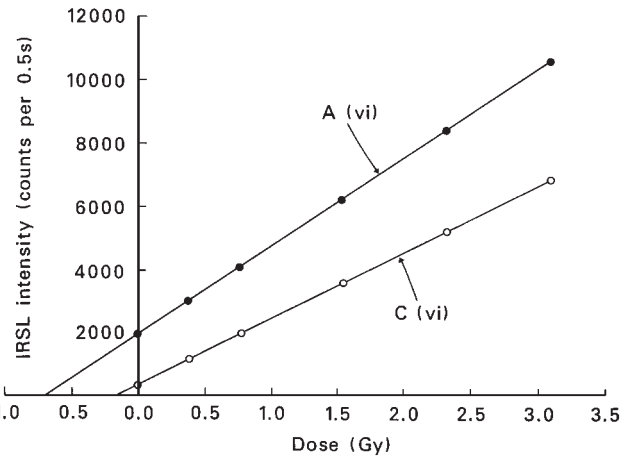

Figure 7 Growth curves for disc 6 (vi) of each of sample A1 and C1, shown without repeat points. Eighteen such runs were performed for each sample and the results are given in Table 3.

Table 3 Single aliquot ED determinations (Gy) and I_n (cts/s) for samples A1 and C1 (actual measurements in 0.5 s have been multiplied by 2)

Disc No.	A1		C1	
	ED ± σ	I_n	ED ± σ	I_n
1	0.97 ± 0.12*	4886	0.22 ± 0.03	508
2	0.85 ± 0.04	3674	0.17 ± 0.02	676
3	0.70 ± 0.02	2592	0.16 ± 0.01	544
4	0.79 ± 0.03	4138	0.17 ± 0.02*	574
5	0.94 ± 0.04*	4636	0.23 ± 0.03	662
6	0.68 ± 0.02	3904	0.15 ± 0.01	596
7	0.77 ± 0.05	3782	0.21 ± 0.02	804
8	0.73 ± 0.05	3792	0.15 ± 0.01*	738
9	0.76 ± 0.05	3152	0.18 ± 0.02	846
10	0.83 ± 0.05	4776	0.19 ± 0.01	720
11	0.79 ± 0.03	3950	0.17 ± 0.01	668
12	0.75 ± 0.03	3776	0.20 ± 0.03	612
13	0.76 ± 0.03	3766	0.18 ± 0.01*	536
14	0.88 ± 0.04*	3940	0.20 ± 0.05	560
15	0.77 ± 0.02	3484	0.18 ± 0.02	758
16	0.80 ± 0.05	3142	0.19 ± 0.02	576
17	0.81 ± 0.03	3554	0.17 ± 0.01	620
18	0.85 ± 0.04	4040	0.17 ± 0.01	778

*Omitted in mean ED used in age calculation.

up in the scatter of the individual data points used to construct the additive dose growth curve. This would have resulted in a similar error term for the ED for that approach.

Another advantage of the single aliquot method is the extra information that can be derived from a data set made up of 18 EDs and related initial signal intensities, I_n. For identical subsamples the values of ED and I_n should be the same, and plots of ED versus I_n which do not form a tight cluster can provide information about the luminescence properties of the grains which make up each subsample (Clarke, 1996). This approach was first used by Li (1994) to identify the inclusion of poorly bleached grains of feldspars obtained from colluvial deposits. Figure 8 shows four plots of normalized ED versus normalized I_n, for samples A1 and C1 representing the oldest and youngest samples in the present set and for samples B6 and B3, both from the same dune spine (Table 4). The data were normalized to the mean of the ED and I_n, giving $(ED)_N$ and $(I_n)_N$ (Table 5). For samples with identical sensitivity and identical past radiation history, the data set would form a single point at (1,1). For samples with the same ED, spread along the horizontal axis indicates that the grains on the discs have different sensitivities, whereas the lack of spread in $(ED)_N$ indicates that all grains have a similar ED; the data for B6 show this behaviour. This implies that all the grains had the same residual dose (probably zero) at deposition. An $(ED)_N$ versus $(I)_N$ plot with a slope of 1 would be given if the grains had the same sensitivity but different radiation histories, giving a variable signal intensity due to the variable ED; the data for sample A1 show a consistent spread in $(ED)_N$ and $(I)_N$ (Figure 8), resulting in a linear trend. This would also be expected if the grains contained different residual doses at deposition. For B3, the scatter in $(I_n)_N$ is similar to that for B6, but that for $(ED)_N$ is many times greater and may indicate that not all grains were totally bleached at deposition.

Results

Tables 1 and 2 show details of analytical calculations and age determinations for the 18 samples from Inch. The error term cited for the ED is given as ± the standard deviation. The ages shown in Table 2 are unrounded.

The largest standard deviation in the ED values obtained was 0.07 Gy for sample B3, corresponding to an uncertainty of 24%. Combining this standard deviation with the dose rate for the sample results in an age uncertainty of 50 years. For the samples with the smallest standard deviation (C1 and D1) of 0.02 Gy, the age uncertainty is calculated as 15 years. The mean value of the standard deviation in the ED for all 18 samples is 0.04 Gy, corresponding to about 30 years, with there being no difference between the values for the dune samples or those from the beach. The standard deviation, rather than the statistical error, is used for the age calculation since, even though the data sets represent at least 15 independent measurements, they would not be measuring the same ED if each had a different dose.

Another reason for the scatter could be the different microdosimetry. This might be due to variations in the external dose rate to the grains, caused for example by the presence of occasional

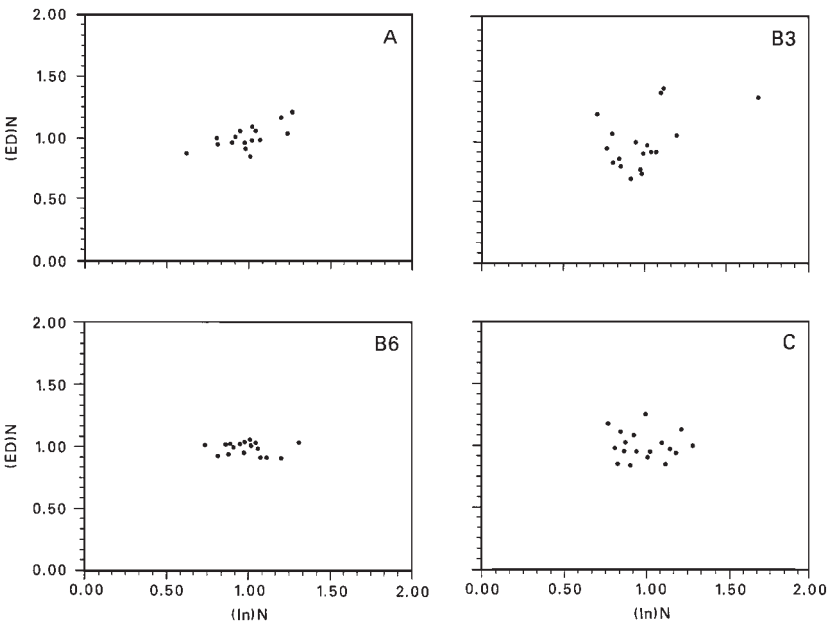

Figure 8 Plots of normalized equivalent dose $(ED)_N$ versus normalized natural intensity $(I_n)_N$ for four samples, the oldest (A1), the youngest (C1), and two from dune transect B.

Table 4 Equivalent dose ED (Gy) and natural intensity I_n (cts/0.5 s) for four samples, A1, B3, B6 and C1) giving the mean (χ) and standard deviation (σ_{n-1}) and the standard deviation from the mean

Aliquot number	A		B3		B6		C	
	ED	I_n	ED	I_n	ED	I_n	ED	I_n
1	0.972	2443	0.426	1400	0.478	2546	0.216	254
2	0.848	1837	0.317	1010	0.479	2462	0.174	338
3	0.705	1216	0.281	966	0.546	3006	0.156	272
4	0.788	2069	0.254	1060	0.547	2242	0.174	287
5	0.935	2318	0.416	1380	0.501	2222	0.230	331
6	0.683	1952	0.364	894	0.542	2178	0.153	298
7	0.770	1891	0.229	1226	0.543	2386	0.206	402
8	0.733	1896	0.272	1306	0.535	1692	0.155	369
9	0.760	1576	0.311	1502	0.528	2086	0.183	423
10	0.833	2388	0.205	1144	0.558	2316	0.187	360
11	0.785	1975	0.405	2120	0.518	2422	0.166	334
12	0.754	1888	0.218	1228	0.532	2340	0.198	306
13	0.763	1883	0.287	1274	0.541	2040	0.178	268
14	0.878	1970	0.268	1242	0.538	1980	0.203	280
15	0.775	1742	0.246	1012	0.488	1862	0.177	379
16	0.802	1571	0.235	1070	0.480	2754	0.187	288
17	0.806	1777	0.272	1344	0.496	2008	0.174	310
18	0.850	2020	0.296	1184			0.172	389
χ	0.802	1912	0.295	1242	0.521	2267	0.183	327
σn−1	0.074	269	0.068	274	0.027	324	0.021	50
S_N	0.093	0.155	0.229	0.221	0.053	0.143	0.116	0.154

Table 5 Normalized equivalent dose $(ED)_N$ and natural intensity $(In)_N$ for same four samples as in Table 4, as plotted in Figure 8

Aliquot number	A		B3		B6		C	
	$(ED)_N$	$(In)_N$	$(ED)_N$	$(In)_N$	$(ED)_N$	$(In)_N$	$(ED)_N$	$(In)_N$
1	1.212	1.278	1.444	1.127	0.917	1.119	1.180	0.777
2	1.057	0.961	1.075	0.813	0.919	1.092	0.951	1.034
3	0.879	0.636	0.953	0.778	1.048	1.321	0.852	0.832
4	0.983	1.082	0.861	0.853	1.050	0.985	0.951	0.878
5	1.166	1.212	1.410	1.111	0.962	0.976	1.257	1.012
6	0.852	1.021	1.234	0.720	1.040	0.957	0.836	0.911
7	0.960	0.989	0.776	0.987	1.042	1.048	1.126	1.229
8	0.914	0.992	0.922	1.052	1.027	0.743	0.847	1.128
9	0.948	0.824	1.054	1.209	1.013	0.917	1.000	1.294
10	1.039	1.249	0.695	0.921	1.071	1.018	1.022	1.101
11	0.979	1.033	1.373	1.707	0.994	1.064	0.907	1.021
12	0.940	0.987	0.739	0.989	1.021	1.028	1.082	0.936
13	0.951	0.985	0.973	1.026	1.038	0.896	0.973	0.820
14	1.095	1.030	0.908	1.000	1.033	0.870	1.109	0.856
15	0.966	0.911	0.834	0.815	0.937	0.818	0.967	1.159
16	1.000	0.822	0.797	0.862	0.921	1.210	1.022	0.881
17	1.005	0.929	0.922	1.082	0.952	0.882	0.951	0.948
18	1.060	1.056	1.003	0.953			0.940	1.190

grains of high radioactive content, such as zircons. Alternatively it could be due to variations in internal dose rate from potassium within the grains, i.e. not all the grains have the average potassium content which was determined for 100 mg of the separated grains. Once again the standard deviation is the more appropriate error term for the age calculation.

Discussion

It is possible to use the data in Tables 3 and 4 to comment on the possibility of individual samples containing grains which had not been totally bleached at deposition. Using the approach of Clarke (1996), the standard deviation of each aliquot from the mean, $S_N = \sigma_{n-1}/\chi$ is calculated, where χ is the mean ED and σ_{n-1} is the standard deviation. Plotting S_N (as a percentage) determined for each sample against χ (the value used in the age calculation), it is evident that there is a trend of increasing scatter with decreasing ED (Figure 9).

The most likely explanation for the higher scatter for the lower EDs is variation in the residual level at deposition. Huntley and Berger (1995) have discussed the causes of scatter in IRSL signals from potassium feldspar separates extracted from young sediments, but only in respect of the multiple aliquot procedure. For

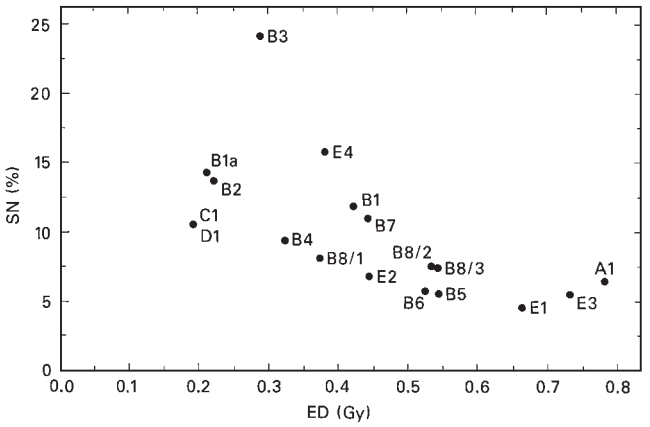

Figure 9 Plot of the standard deviation from the mean expressed as a % versus ED (Gy) for each sample taken from penultimate column of Table 2.

older samples the variable residual level becomes less important. Observation of this trend was not expected, as work by others on modern samples has not suggested that there is a finite lower age limit. Using the same method, but in a desert environment, Edwards (1993) obtained an age as low as 40 ± 15 yrs and Ollerhead *et al.* (1994) in a similar environment obtained an age of 5 ± 30 yrs using a multiple aliquot approach.

The ages presented in Table 2 were calculated from the mean value of the ED and its standard deviation, using no less than 15 individual ED determinations. However, this is not the only source of uncertainty in the error on the age. The random and systematic errors for each of the dose rate measurements are also combined into the final error assessment (Aitken, 1985: 242).

Two sources of uncertainty of particular relevance at this site are the water content and the cosmic dose rate. Uncertainty in the water content, due to past fluctuations in the water table or proximity to the surface of the dune, will always place limits on the precision of the calculated total dose rate and thus on the ages obtained, but for dune samples the past water content can be assessed fairly precisely from current water content measurements and laboratory measurements of saturation water contents. The values used in the age calculation are compatible with the value of 8 ± 3% assumed by Ollerhead *et al.* (1994) for their samples which were all taken within about 0.6 m of the water table. For the samples from the beach face, a water content of 30 ± 10% was assumed, and this alone results in a 10% uncertainty in the age (Aitken, 1985: 243).

For samples from the side walls of the dune alleyways it was possible to measure the thickness of the overlying sediment for incorporation into the equation for the cosmic dose rate (Prescott and Hutton, 1988). However, for the samples from the base of the alleyways, a time-averaged thickness of overlying sand had to be estimated. For all the dune samples, a 10% uncertainty in the cosmic dose rate was applied, to allow for dune build-up and removal.

In spite of the foregoing discussion, the age determinations are consistent with the relative ages based on the geomorphological position of the samples, e.g. the age of the vertical dune face on the seaward limit of the dune field (B5–B2: 368–151 yr. BP) shows conformity of dates and deposition. The maximum age of sand emplacement is 600–500 yrs, as found at the landward end of the spit. We note the clustering of ages *c*. 150 yr ago for samples that are taken from within three parabolic alleyways (B1A, C1 and D1); this second phase of activity might be correlated with a major event, i.e. the 'Big Wind' of 1839 (Carr, 1993), or with anthropogenic pressure on the dunes during times of land-eviction.

Conclusion

This is the first study to apply IRSL dating to dunes from western Ireland and has provided the opportunity to investigate the viability of dating very young dunes. Although the ages for the four youngest samples (B1a, B2, C1 and D1) permit us to associate them with an historically documented storm, the higher degree of scatter in their ED values may indicate the presence of grains with different residual signals at deposition.

The remaining luminescence dates show that there has been substantial sand mobilization and deposition during the last 600 years, both in the dunes and in the beach face associated with sediment storage prior to transfer into the dunes. There is an absence of luminescence dates for sediments between the youngest gravels at *c*. 1100 BP and this major phase of sand deposition starting at 600–500 yr. BP. However, no samples were taken from the sand unit directly above the gravel. The ^{14}C age of the midden shells is consistent with the luminescence age of the parabolic dune.

Acknowledgements

The analytical work was funded under CEC Environment and Climate programme grant EV5V-CT93–0266. We wish to acknowledge the help of John McKenna, Cathy Delaney and Robert Stewart in determining the horizontal and vertical position of samples used in this dating study, Kate Richardson and Susanna Valencio for field assistance and Andrew Warren for his critical review of the manuscript.

References

Aitken, M.J. 1985: *Thermoluminescence dating*. London: Academic Press.

Bøtter-Jensen, L. and **Mejdahl, V.** 1985: Determination of potassium in feldspars by beta counting using a GM multicounter system. *Nuclear Tracks and Radiation Measurements* 10, 663–66.

Carr, P. 1993: *The night of the big wind* (second edition). Belfast: White Row Press.

Carter, R.W.G. 1990: The geomorphology of coastal dunes in Ireland. In Bakker, Th.W.M., Jungerius, P.D. and Klijn, J.A., editors, *Dunes of the European coasts, Catena Supplement* 18, 31–39.

Carter, R.W.G., Devoy, R.J.N. and **Shaw, J.** 1989: Late Holocene sea levels in Ireland. *Journal of Quaternary Science* 4, 7–24.

Clarke, M.L. 1994: Infra-red stimulated luminescence ages from aeolian sand and alluvial fan deposits from the eastern Mojave Desert, California. *Quaternary Geochronology (Quaternary Science Reviews*) 13, 533–38.

— 1996: IRSL dating of sands: bleaching characteristics at deposition using single aliquots. *Radiation Measurements* 26(3), 611–20.

Clarke, M.L., Wintle, A.G. and **Lancaster, N.** 1996: Infra-red stimulated luminescence dating of sands from the Cronese Basin. *Geomorphology* 17, 199–205.

Duller, G.A.T. 1991: Equivalent dose determination using single aliquots. *Nuclear Tracks and Radiation Measurements* 18, 371–78.

— 1995: Luminescence dating using single aliquots: methods and applications. *Radiation Measurements* 24, 217–26.

Edwards, S.R. 1993: Luminescence dating of sand from the Kelso Dunes, California. In Pye, K., editor, *The dynamics and environmental context of aeolian sedimentary systems*. London: Geological Society, Special Publication No. 72, 59–68.

Huntley, D.J. and **Berger, G.W.** 1995: Scatter in luminescence data for optical dating some models. *Ancient TL* 13, 5–8.

Li, S.H. 1994: Optical dating: insufficiently bleached sediments. *Radiation Measurements* 23, 563–67.

Nambi, K.S.V. and **Aitken, M.J.** 1986: Annual dose conversion factors for TL and ESR dating. *Archaeometry* 28, 202–205.

Ollerhead, J. and **Davidson-Arnott, R.G.D.** 1995: The evolution of Buctouche Spit, New Brunswick, Canada. *Marine Geology* 124, 215–36.

Ollerhead, J., Huntley, D.J. and **Berger, G.W.** 1994: Luminescence dating of sediments from Buctouche Spit, New Brunswick. *Canadian Journal of Earth Sciences* 31, 523–31.

Prescott, J.R. and **Hutton, J.T.** 1988: Cosmic ray and gamma ray dosimetry for TL and ESR. *Nuclear Tracks and Radiation Measurements* 14, 223–27.

Pye, K., Stokes, S. and **Neal, A.** 1995: Optical dating of aeolian sediments from the Sefton coast, northwest England. *Proceedings of the Geologists' Association* 106, 281–92.

Sanderson, D.C.W. 1988: Thick source beta counting (TSBC): a rapid method for measuring beta dose rates. *Nuclear Tracks and Radiation Measurements* 14, 203–207.

Stokes, S. 1992: Optical dating of young (modern) sediment using quartz: results from a selection of depositional environments. *Quaternary Science Reviews* 11, 153–59.

Stokes, S. and **Gaylord, D.R.** 1993: Optical dating of Holocene dune sands in the Ferris dunefield, Wyoming. *Quaternary Research* 39, 274–81.

Wintle, A.G. 1993: Luminescence dating of aeolian sands: an overview. In Pye, K., editor, *The dynamics and environmental context of aeolian sedimentary systems*, London: Geological Society, Special Publication No. 72, 49–58.